Journal of Elasticity **33**: 259–293, 1993.

On higher order gradient continuum theories in 1-D nonlinear elasticity. Derivation from and comparison to the corresponding discrete models

N. TRIANTAFYLLIDIS and S. BARDENHAGEN

College of Engineering, Department of Aerospace Engineering, The University of Michigan, Ann Arbor, Michigan 48109-2140, USA

Received 7 November 1991; in revised form 3 May 1993

Abstract. Higher order gradient continuum theories have often been proposed as models for solids that exhibit localization of deformation (in the form of shear bands) at sufficiently high levels of strain. These models incorporate a length scale for the localized deformation zone and are either postulated or justified from micromechanical considerations. Of interest here is the consistent derivation of such models from a given microstructure and the subsequent comparison of the solution to a boundary value problem using both the exact microscopic model and the corresponding approximate higher order gradient macroscopic model.

In the interest of simplicity the microscopic model is a discrete periodic nonlinear elastic structure. The corresponding macroscopic model derived from it is a continuum model involving higher order gradients in the displacements. Attention is focused on the simplest such model, namely the one whose energy density involves only the second order gradient of the displacement. The discrete to continuum comparisons are done for a boundary value problem involving two different types of macroscopic material behavior. In addition the issues of stability and imperfection sensitivity of the solutions are also investigated.

1. Introduction

A common feature among ductile solids, when sufficiently strained, is the transition from a smoothly varying deformation field into a highly localized deformation pattern in the form of a "shear band". This local, i.e. appearing at any point whose stress state reaches a critical level, instability phenomenon is modeled within the framework of continuum mechanics as a loss of ellipticity in the incremental equilibrium equations. This approach has been proposed in the context of elasticity by Hadamard [17] and subsequently for rate independent elastoplasticity by Thomas [31], Hill [18] and Mandel [24]. The characteristic surfaces of the governing equations indicate the position of the localized deformation zones. Considerable effort has been subsequently devoted to the study of the localization of deformation's dependence on the assumed constitutive model. For further information on this subject, the interested reader is referred to Knowles and Sternberg [20] for elastic materials and Rice [29] for inelastic ones.

The loss of ellipticity approach is adequate for predicting the critical stress

level and deformation zone direction at the onset of localized deformation. However, it can neither predict the size of the localized deformation zone nor can it provide any constitutive information about the evolution of deformation inside the zone. Due to these limitations, numerical (usually finite element) calculations in related boundary value problems show an undesirable dependence of results on selected mesh size and orientation (see Tvergaard, Needleman and Lo [35]).

Motivated by the above physical and numerical shortcomings of the simple loss of ellipticity approach, and in view of the increased importance of analyzing localized failure phenomena in mechanics, a number of remedies have been proposed. In the classical continuum mechanics framework, these improvements consist of either the consideration of imperfection sensitivity to pre-existing weak zones in the solid (see Marciniak and Kuczynski [25]), or the incorporation in the constitutive model of viscous or thermal coupling effects (see Molinari and Clifton [28], Clifton [12]). The non-classical continuum mechanics alternative consists of relaxing the local action hypothesis, according to which the strain depends only on the first gradient of the deformation. Continuum models that violate the local action hypothesis are termed non-local. They are divided into two categories: The first category consists of integral models with strains and stresses at a given point depending on a convolution type integral that accounts for the history of displacements in a finite neighborhood about the point in question. The second category consists of higher order gradient models for which the strains and stresses at a point depend on the history of all the gradients of the displacement – up to a certain order – at that particular point.

Of interest here is the last approach to modeling the localization of deformation, namely the incorporation of higher order gradients in the constitutive law. Among the attractions of this approach are its simplicity (no dependence on unknown "weak zones" in the solid or difficult to determine influence functions for the convolution integrals appearing in integral type non-local models, no time or temperature effects required) and the inherent existence of a characteristic length scale in the model that determines the size of the localized deformation zones which appear at adequately large levels of strain. More specifically, constitutive models that incorporate up to the second gradient of deformation are the simplest such models that exhibit the wanted localized strain solutions with zone widths that depend on the characteristic length scale. The incorporation of a second order gradient term in the material law found many applications in the study of localization phenomena, not only for solids (see Aifantis [6], Coleman [13], Coleman and Hodgdon [14]) but in fluids as well (see Van der Waals [36] classical 1893 paper and also Aifantis and Serrin [4, 5]).

The above-mentioned constitutive models, although often physically moti-

vated, are essentially phenomenological. The coefficients of the second order gradient terms are either postulated (as in Triantafyllidis and Aifantis [34]) or heuristically derived from the assumption of continuum state equations coupling macroscopic and microscopic state variables (see Mindlin [26], Eringen and Suhubi [15], Suhubi and Eringen [30], Aifantis [7]). With the recent considerable growth of higher order gradient models proposed for an ever increasing number of material behaviors, e.g. elastoplastic, viscoplastic, thermoviscoplastic, the issues of consistent derivation of the macroscopic model from the microscale one and comparison of the solutions to the same boundary value problem for the two corresponding models, become increasingly relevant.

For simplicity, attention will be here restricted only to one-dimensional nonlinear elastic media with arbitrary periodic microstructure. Of interest is the consistent derivation of the macroscopic higher order gradient continuum model from the properties of the discrete microstructure. Also of interest is the comparison of solutions to boundary value problems using alternatively the exact discrete micro model and the corresponding approximate continuum macro model. Although derivations of higher order gradient continuum theories based on discrete periodic microstructures are not novel, especially in the Physics literature (see for example Askar [9], Kunin [21], Mindlin [27], Toupin and Gazis [32]), attention has been focused on linear theories, static or dynamic. The derivation of higher order gradient continuum theories from the nonlinear periodic microstructures of interest here does not seem to have attracted attention so far, to the best of the authors' knowledge. The same comment applies to the comparison between the continuum and discrete solutions to boundary value problems for the above discussed microstructures.

The outline of this paper is as follows: Section 2 details the general discrete periodic elastic model and briefly outlines the numerical solution procedure. Section 3 outlines the derivation, using two different approaches, of the continuum macro model from the properties of the discrete periodic micro model. The analytical solution to the boundary value problem for the continuum model is also derived. Section 4 presents two particular discrete models and the discrete vs. continuum comparisons. The force-displacement diagrams and the equilibrium strain profiles for the localized solutions are compared, and the stability of the solutions is studied. Section 5 concludes the presentation with a discussion of the results.

2. The discrete model

2.1. Description

Consider a one-dimensional structure composed of equally spaced nodes connected by nonlinear elastic springs. The node spacing is denoted by ε, and

the total length of the structure is $L = N\varepsilon$ with $N + 1$ the total number of nodes. A typical node, say i, is connected to all the adjacent nodes j with $i - q \leqslant j \leqslant i + q$ where q is an integer indicating the maximum number of neighboring nodes to which each node is connected on each side (see Fig. 2.1 where $q = 2$). The force (f)–strain (e) relation for a spring of length $p\varepsilon$ $(1 \leqslant p \leqslant q)$ is denoted by $f_p(e_p)$, while the corresponding stored energy in the spring is $p\varepsilon w_p(e_p)$ with $w_p' = f_p$.

The strain e_p in a spring of length $p\varepsilon$ attached to node i is given by

$$e_p^{i+} = \frac{u_{i+p} - u_i}{p\varepsilon} \quad \text{or} \quad e_p^{i-} = \frac{u_i - u_{i-p}}{p\varepsilon}, \tag{2.1}$$

where e_p^{i+} and e_p^{i-} are the strains in the springs at the right of node i and at the left of node i respectively. Here u_j denotes the total displacement of node j.

The kinematical definitions in (2.1) are valid for nodes sufficiently far from the end nodes of the structure, i.e. for $0 \leqslant i - q$ and $i + q \leqslant N$. To ensure a trivial equilibrium solution $\overset{0}{u}_i$ of equal relative displacements (i.e. $\overset{0}{u}_{i+1} - \overset{0}{u}_i = \text{const}$), the following kinematical relations for e_p^{i+} and e_p^{i-} are adopted:

$$e_p^{i+} = \frac{2u_N - u_{2N-i-p} - u_i}{p\varepsilon} \quad \text{for } i + p > N,$$

$$e_p^{i-} = \frac{u_i + u_{p-i} - 2u_0}{p\varepsilon} \quad \text{for } i - p < 0. \tag{2.2}$$

The above relations are derived from the tacit assumption of the existence of fictitious outside nodes $i < 0$ and $i > N$ whose relative displacements with respect to the end nodes 0 and N are mirror images of the relative displacements of the corresponding mirror interior nodes.

The equilibrium equation for interior node i $(0 < i < N)$, assuming that no

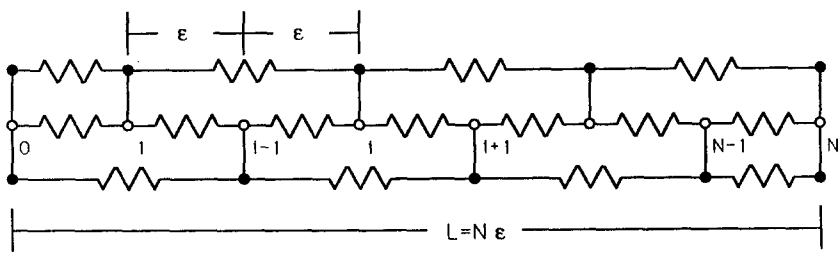

Fig. 2.1. Schematic diagram of the discrete nonlinear elastic periodic model for $q = 2$.

external forces are applied, is given by

$$\sum_{p=1}^{q} [f_p(e_p^{i+}) - f_p(e_p^{i-})] = 0. \tag{2.3}$$

The selection of the force-strain relation $f_p(e_p)$ for each spring of length $p\varepsilon$ will be specified and explained in Section 4.

2.2. Setting of the boundary value problem

The one-dimensional structure described above with $N + 1$ nodes is held fixed at node 0 ($u_0 = 0$) and is subject to an end displacement Δ at node N ($u_N = \Delta$). The $N - 1$ equilibrium equations (2.3) ($i = 1, \ldots, N - 1$) for the $N - 1$ unknown displacements $(u_1, \ldots, u_{N-1})$ are solved numerically using a straightforward incremental Newton-Raphson technique.

A trivial solution to the problem, which is also termed the principal or the prebifurcated solution and is denoted by $\overset{0}{u}_i$, corresponds to a uniform straining of the structure with $\overset{0}{u}_i = i\varepsilon\overset{0}{e}$. As is easily verified from the kinematic relations (2.1), (2.2) the corresponding strain within each spring is $\overset{0}{e}_p^{i+} = \overset{0}{e}_p^{i-} = \overset{0}{e} = \Delta/L$ and thus the equilibrium equation (2.3) is satisfied at all the interior nodes. To summarize

$$\overset{0}{u}_i = i\varepsilon\overset{0}{e}, \quad \overset{0}{e} = \Delta/L, \quad \overset{0}{e}_p^{i+} = \overset{0}{e}_p^{i-} = \overset{0}{e}. \tag{2.4}$$

The above solution is valid for any value of the end displacement Δ. For adequately small values of Δ the principal solution (2.4) is unique and stable through an appropriate choice of the $f_p(e_p)$. The properties of the nonlinear springs in the model will be chosen so that when Δ exceeds a critical value, the (uniform strain) principal solution is no longer unique; other equilibrium branches, termed the bifurcated equilibrium branches, emerge from the principal solution. The strains in these bifurcated branches are no longer equal for each spring, but increase in a small neighborhood of the structure while remaining approximately uniform but decreasing in the remaining part of the structure. Because of this property, the bifurcated solutions will also be termed the localized strain solutions. The localized strain (bifurcated) equilibrium solutions are studied in detail in Section 4.

3. The continuum approximation

When the node spacing $\varepsilon \to 0$ (or equivalently the number of nodes $N \to \infty$) the discrete system of algebraic equations (2.1)–(2.3) can be approximated by a

differential equation for $u(x)$ where $u_i \cong u(x_i)$ and the coordinate $x_i = i\varepsilon$. Finding the appropriate differential equation whose solution approaches the solution for the discrete system is a classical problem that occurs in many branches of mathematical physics. Of particular interest here is the consistent derivation of the simplest higher order gradient continuum model whose energy density per unit length is postulated to be (see Triantafyllidis and Aifantis [34])

$$\widehat{W} = W(u_{,x}) + \tfrac{1}{2}\varepsilon^2 h(u_{,x})[u_{,xx}]^2. \tag{3.1}$$

To find the relations between $W(u_{,x})$, $h(u_{,x})$ of the continuum model and the properties of the discrete model (i.e. $f_p(e_p)$), two different approaches are used: The first approach uses as a departing point the discrete equilibrium equation at node i (2.3) to arrive at a corresponding continuum equation which in turn can be identified as the Euler-Lagrange equation of an energy functional of the form (3.1). The second approach proceeds directly with the derivation of a continuum energy from the energies of all springs attached to node i. Both approaches lead to the same Euler-Lagrange (equilibrium) equation.

It should be noted at this point that the ensuing derivations provide a continuum energy density up to any order of ε required. Only the lowest order correction in the energy, i.e. the $O(\varepsilon^2)$ term is of interest here, for it brings up the effect of the microstructure in the simplest way. In Section 4 the solution to the boundary value problem for the discrete model described in Section 2 will be compared with the solution to the same boundary value problem for the corresponding continuum with energy density in the form (3.1).

3.1. Continuum model derivation via equilibrium

Consider the equilibrium of an interior node i away from the boundary of the discrete model. An adequately smooth continuous function $u(x)$ is assumed that coincides with all the equilibrium displacements u_j at nodal points $x_j = j\varepsilon$. Using the Taylor series expansion about x_i to evaluate the strains e_p^{i+}, e_p^{i-} in all the nonlinear springs that affect the equilibrium of node i, one has from (2.1)

$$\begin{aligned} e_p^{i+} &= \frac{u_{i+p} - u_i}{p\varepsilon} = u_{,x} + \frac{1}{2}\, p\varepsilon u_{,xx} + \frac{1}{6}\,(p\varepsilon)^2 u_{,xxx} + \frac{1}{24}\,(p\varepsilon)^3 u_{,xxxx} + \cdots, \\ e_p^{i-} &= \frac{u_i - u_{i-p}}{p\varepsilon} = u_{,x} - \frac{1}{2}\, p\varepsilon u_{,xx} + \frac{1}{6}\,(p\varepsilon)^2 u_{,xxx} - \frac{1}{24}\,(p\varepsilon)^3 u_{,xxxx} + \cdots, \end{aligned} \tag{3.2}$$

where all derivatives of $u(x)$ are evaluated at x_i.

Substitution of (3.2) into the equilibrium equation (2.3) and subsequent

expansion of the result in terms of ascending powers of ε yields

$$\sum_{p=1}^{q} p \left\{ f_p'(u_{,x})u_{,xx} + \frac{(p\varepsilon)^2}{6} \left[f_p'''(u_{,x}) \frac{u_{,xx}^3}{4} + f_p''(u_{,x})u_{,xx}u_{,xxx} + f_p'(u_{,x}) \frac{u_{,xxxx}}{2} \right] + O(p\varepsilon)^4 \right\} = 0, \tag{3.3}$$

where $(\,)'$ denotes derivation of a function with respect to its argument.

By inspection, one finds (3.3) to be the Euler-Lagrange (equilibrium) equation of the functional $\int_0^L \widehat{W}(u_{,x}, u_{,xx}, \ldots)\,\mathrm{d}x$, where

$$\widehat{W} = \sum_{p=1}^{q} p w_p(u_{,x}) + \frac{\varepsilon^2}{2} \left\{ \left[-\sum_{p=1}^{q} \frac{p^3}{12} w_p''(u_{,x}) \right] (u_{,xx})^2 \right\} + O(\varepsilon^4) \tag{3.4}$$

with $w_p(e_p)$ the energy density of a spring of length $p\varepsilon$ (recall $w_p' = f_p$).

Comparison of (3.1) and (3.4) gives

$$W(u_{,x}) = \sum_{p=1}^{q} p w_p(u_{,x}) \quad \text{and} \quad h(u_{,x}) = -\sum_{p=1}^{q} \frac{p^3}{12} w_p''(u_{,x}),$$

which are the wanted relations linking the phenomenological macroscopic (continuum) energy density (3.1) to the corresponding microscopic (discrete) model.

3.2. Continuum model derivation via energy

The energy per unit length of the discrete structure, say $\overline{W}$, equals half of the energy of all springs connected to a sufficiently distant from the boundary interior node i, divided by the nodal spacing ε, i.e.

$$\overline{W} = \frac{1}{2\varepsilon} \sum_{p=1}^{q} \left[p\varepsilon w_p(e_p^{i^+}) + p\varepsilon w_p(e_p^{i^-}) \right], \tag{3.5}$$

Substitution of the strains $e_p^{i^+}$ and $e_p^{i^-}$ in terms of $u(x)$ and its derivatives at x_i according to (3.2) gives, after a straightforward expansion in terms of ascending powers of ε

$$\overline{W} = \sum_{p=1}^{q} p w_p(u_{,x}) + \frac{\varepsilon^2}{2} \left\{ \sum_{p=1}^{q} p^3 \left[w_p''(u_{,x}) \frac{(u_{,xx})^2}{4} + w_p'(u_{,x}) \frac{u_{,xxx}}{3} \right] \right\} + O(\varepsilon^4). \tag{3.6}$$

Notice that although the $O(\varepsilon^0)$ term in (3.6) coincides with its counterpart in (3.4), this is not the case with the $O(\varepsilon^2)$ term (or any higher order term). This discrepancy does not affect equilibrium, since the Euler-Lagrange equation for the functional $\int_0^L \overline{W}\, dx$ coincides with (3.3) as a straightforward calculation can verify. The boundary conditions are in general different. For the displacement controlled boundary value problem considered here, one can easily show that the boundary conditions are satisfied for either energy density. Moreover, the same calculation shows that the end force dependence on the displacement field is also unaffected by the energy density choice.

The fact that more than one continuum energy density can be found for the same discrete model is a known complication in mathematical physics (see for example the discussion in Kunin [21]). The various continuous energies differ by a null Lagrangian, i.e. a functional whose Euler-Lagrange differential equation is identically zero. For the model at hand this means that the functional $\int_0^L (\widehat{W} - \overline{W})\, dx$ is a null Lagrangian, which implies that each term in ε is a null Lagrangian. One can easily verify that the $O(\varepsilon^2)$ term of the above differences in energy $(=(1/2)\int_0^L \Sigma_{p=1}^{q} (p^3/3)[w_p''(u_{,x})u_{,xx}^2 + w_p'(u_{,x})u_{,xxx}])$ has an Euler-Lagrange equation that vanishes identically. This property is also shared by all the higher order in ε terms in the above-mentioned energy difference, as a tedious but straightforward calculation can verify.

3.3. *Setting of the boundary value problem*

The one-dimensional continuum model has energy density $\widehat{W}$ given by (3.1) and is of length L. This energy density is preferred over $\overline{W}$ in view of its simpler form and also on account of its frequent use in previous investigations. In accordance with the boundary value problem for the discrete model (see Section 2.2) the end displacements of the continuum model are prescribed, i.e. $u(0) = 0$, $u(L) = \Delta$. The model's potential energy, in the absence of body forces, is

$$\mathscr{E}(u, \Delta) = \int_0^L \left\{ W(u_{,x}) + \frac{\varepsilon^2}{2} h(u_{,x})[u_{,xx}]^2 \right\} dx.$$

The equilibrium equation (3.7) and the natural boundary conditions $(3.8)_1$ are found by extremizing $\mathscr{E}$ over all admissible displacements $u(x)$ (i.e. all continuously differentiable functions $u(x)$ that satisfy the above-mentioned essential boundary conditions). A standard calculation from $\mathscr{E}_{,u}\delta u = 0$ gives

$$W'(u_{,x}) - \varepsilon^2 u_{,xxx} h(u_{,x}) - \frac{\varepsilon^2}{2}[u_{,xx}]^2 h'(u_{,x}) = c, \tag{3.7}$$

$$u_{,xx}(0) = u_{,xx}(L) = 0, \tag{3.8}_1$$

$$u(0) = 0, \quad u(L) = \Delta. \tag{3.8}_2$$

The constant c in (3.7) is the force exerted at the ends of the structure and is constant throughout the structure, in view of the absence of body forces. The system of differential equation (3.7) and boundary conditions (3.8) is solved analytically and the solutions are presented and discussed in detail in Section 3.4. As previously noted, had $\overline{W}$ been chosen as the energy density of the continuum model, the corresponding equilibrium equation would be (3.7) and the boundary conditions would be satisfied by (3.8).

As expected from the discrete model (compare with (2.4)), the trivial principal solution $\overset{0}{u}(x)$ to the system (3.7), (3.8) is the uniform strain solution, i.e.

$$\overset{0}{u}(x) = \overset{0}{e}x, \quad \overset{0}{u}_{,x} = \overset{0}{e} = \Delta/L, \quad W'(\overset{0}{e}) = c. \tag{3.9}$$

The above solution is valid for any value of Δ. When Δ exceeds a certain critical value, bifurcated equilibrium branches emerge from the principal solution, exactly as in the discrete model. The bifurcated branches have, as expected, solutions in which the strain $u_{,x}$ is localized around a narrow zone. The comparison of the localized strain solutions of the continuum model boundary value problem to the localized strain solutions of the discrete model boundary value problem is the main task of Section 4.

3.4. Solution of the continuum boundary value problem

As discussed in Triantafyllidis and Aifantis [34], the essential features of the continuum energy density $\widehat{W}$, which are responsible for the appearance of localized strain solutions, are:

(i) A macroscopic behavior that presents a maximum in the corresponding stress–strain curve, i.e. a twice differentiable, smooth macroscopic energy density $W(u_{,x})$ with the properties

$$W(0) = W'(0) = 0,$$

$$W''(u_{,x}) > 0 \quad \text{for } 0 \leqslant u_{,x} < e_m, \quad W''(e_m) = 0. \tag{3.10}$$

The physical interpretation of (3.10) is that the macroscopic stress–strain relation $W'(u_{,x}) - u_{,x}$ attains a maximum at $u_{,x} = e_m$. This feature is responsible for the existence of discontinuous strain gradient solutions in models where the effects of microstructure are ignored (i.e. when $\widehat{W} = W(u_{,x})$), and

hence responsible for the existence of localized strain solutions when the effects of microstructure are considered (i.e. when $\widehat{W} = W(u_{,x}) + (\varepsilon^2/2)h(u_{,x})[u_{,xx}]^2$).

(ii) An always positive contribution $((\varepsilon^2/2)h(u_{,x})[u_{,xx}]^2)$ to the energy density $\widehat{W}$ due to the microstructural effects, i.e.

$$h(u_{,x}) > 0. \tag{3.11}$$

The above property ensures the absence of discontinuous solutions to the equilibrium equation (3.7) and is responsible for the emergence of bifurcated (localized strain) solutions to the boundary value problem (3.7), (3.8) for average strains larger than e_m, as will be shortly discussed. It also ensures the stability of the uniform strain principal solution for strains ranging from zero past the strain at the macroscopic maximum load e_m up to the first bifurcation. The above condition (3.11) is overly restrictive, for it need not be satisfied for all strains u_x; it suffices to be valid for a neighborhood of e_m. However, this possibility will not be presently explored any further.

3.4.1. Stability of principal solution and bifurcation points

(i) Stability of the principal solution.

To determine the stability of the principal solution (3.9) one must examine the positive definiteness of the functional $(\mathscr{E}_{,uu}(\overset{0}{u}, \Delta)\delta u)\delta u$ (the second Frechet derivative of the structure's energy $\mathscr{E}$) evaluated on the principal branch $\overset{0}{u}(x, \Delta) = \overset{0}{e}x = \Delta x/L$,

$$(\mathscr{E}_{,uu}(\overset{0}{u}, \Delta)\delta u)\delta u = \int_0^L [W''(\overset{0}{e})(\delta u_{,x})^2 + \varepsilon^2 h(\overset{0}{e})(\delta u_{,xx})^2]\,\mathrm{d}x. \tag{3.12}$$

Since all kinematically admissible functions $\delta u(x)$ must satisfy the essential boundary conditions $\delta u(0) = \delta u(L) = 0$ one can without loss of generality take

$$\delta u(x) = \sqrt{2/L} \sum_{n=1}^{\infty} \left[\delta u_n \sin\left(\frac{n\pi x}{L}\right)\right], \tag{3.13}$$

which upon substitution into (3.12) yields

$$(\mathscr{E}_{,uu}(\overset{0}{u}, \Delta)\delta u)\delta u = \sum_{n=1}^{\infty} \left[W''(\overset{0}{e}) + \varepsilon^2 \left(\frac{n\pi}{L}\right)^2 h(\overset{0}{e})\right]\left(\frac{n\pi}{L}\,\delta u_n\right)^2. \tag{3.14}$$

For as long as $W''(\overset{0}{e}) + \varepsilon^2(n\pi/L)^2 h(\overset{0}{e}) > 0$, it follows from (3.14) that the principal solution is stable. As expected for strains $\overset{0}{e} = \Delta/L < e_m$ the stability condition is always satisfied in view of (3.10), (3.11).

Let e_n be the closest to e_m root of

$$W''(e_n) + \varepsilon^2 \left(\frac{n\pi}{L}\right)^2 h(e_n) = 0; \quad n = 1, 2, \ldots. \tag{3.15}$$

Without loss of generality one can assume that $W''(e)/h(e)$ is a monotonically decreasing function of e, in which case $e_m < e_1 < e_2 < \cdots < e_n < \cdots$. Consequently, the first time that an instability is encountered as the displacement Δ increases is at $\Delta_1 = e_1 L$. Notice that the longer the structure, the closer e_1 is to e_m.

(ii) Bifurcation points.

At bifurcation, the critical end displacement Δ_b, strain e_b ($\Delta_b = e_b L$) and corresponding eigenmodes $\overset{b}{u}(x)$ are found from the variational statement

$$(\mathscr{E}_{,uu}(\overset{b}{u}(x, \Delta_b), \Delta_b)\overset{b}{u})\delta u = 0. \tag{3.16}$$

Using (3.9) and taking into account the essential boundary conditions $\overset{b}{u}(0) = \delta u(0) = \overset{b}{u}(L) = \delta u(L) = 0$ results in the following eigenvalue problem: find a solution $\overset{b}{u}(x) \neq 0$ of

$$\varepsilon^2 h(e_b)\overset{b}{u}_{,xxxx} - W''(e_b)\overset{b}{u}_{,xx} = 0, \tag{3.17}$$

$$\overset{b}{u}(0) = \overset{b}{u}_{,xx}(0) = \overset{b}{u}(L) = \overset{b}{u}_{,xx}(L) = 0. \tag{3.18}$$

The solution to the above eigenvalue problem is easily found to be

$$e_b = e_n, \quad \Delta_b = e_n L, \quad \overset{b}{u}(x) = \alpha \sin\left(\frac{n\pi x}{L}\right); \quad n = 1, 2, \ldots, \tag{3.19}$$

where the constants e_n are defined in (3.15), and α is an arbitrary constant (which can be specified if a mode normalization condition is added).

From the above analysis the following characteristics of the principal solution emerge. As the end displacement Δ increases from its zero initial value, the uniform strain solution is stable (i.e. minimizes locally the potential energy) and is devoid of bifurcation points for as long as $\Delta < \Delta_1 = e_1 L$, with e_1 the closest to e_m and thus the smallest root of (3.15). An infinity of bifurcation points Δ_n are encountered after the structure reaches its maximum load (at $\Delta_m = e_m L$) starting with $\Delta_1 > \Delta_m$. These bifurcation points tend all to cluster at Δ_m as the length L of the structure increases.

3.4.2. Bifurcated (localized strain) solutions

The bifurcated equilibrium solutions are found by solving the equilibrium equation (3.7) subject to the boundary conditions (3.8). First the bifurcated solution emerging from $e_1 = \Delta_1/L$, the closest to e_m root of (3.15), will be presented. A simple modification of this solution procedure generates all other bifurcated equilibrium paths, which emerge at higher strains $e_n = \Delta_n/L$, as will be shown subsequently.

By introducing the notation $u_{,x} \equiv e$ for the strain, (3.7) becomes a first order nonlinear ordinary differential equation in $x(e)$, namely

$$W'(e) - \frac{\varepsilon^2}{2}\frac{\mathrm{d}}{\mathrm{d}e}\left[h(e)\left(\frac{\mathrm{d}x}{\mathrm{d}e}\right)^{-2}\right] = c, \quad e \equiv u_{,x}, \tag{3.20}$$

where c is the end force exerted on the structure. Upon integration of (3.20) from e to $e_0 \equiv e(0) = u_{,x}(0)$ and taking into account the natural boundary condition in $(3.8)_1$, $e_{,x}(0) = u_{,xx}(0) = 0$, one obtains

$$x = \varepsilon \int_e^{e_0} \{h(e)/2[W(e) - W(e_0) - c(e - e_0)]\}^{1/2}\,\mathrm{d}e. \tag{3.21}$$

A consequence of the remaining natural boundary condition $e_{,x}(L) = u_{,xx}(L) = 0$ in $(3.8)_1$ and (3.7) is the following expression for c:

$$c = [W(e_0) - W(e_L)]/[e_0 - e_L]; \quad e_L \equiv e(L) = u_{,x}(L), \quad e_0 \equiv e(0) = u_{,x}(0). \tag{3.22}$$

With the help of (3.21) the wanted displacement $u(x) = \int_0^x u_{,x}\,\mathrm{d}x = \int_0^x e\,\mathrm{d}x = \int_{e_0}^{e} e(\mathrm{d}x/\mathrm{d}e)\,\mathrm{d}e$ takes the form

$$u(x) = \varepsilon \int_e^{e_0} e\{h(e)/2[W(e) - W(e_0) - c(e - e_0)]\}^{1/2}\,\mathrm{d}e. \tag{3.23}$$

The unknown values of the strain e_0, e_L at the ends of the structure are found from (3.21) and (3.23) by the requirements $x(e_L) = L$, $u(L) = u(x(e_L)) = \Delta$,

$$L = \varepsilon \int_{e_L}^{e_0} \{h(e)/2[W(e) - W(e_0) - c(e - e_0)]\}^{1/2}\,\mathrm{d}e, \tag{3.24}$$

$$\Delta = \varepsilon \int_{e_L}^{e_0} e\{h(e)/2[W(e) - W(e_0) - c(e - e_0)]\}^{1/2}\,\mathrm{d}e. \tag{3.25}$$

Hence the sought bifurcated solution $u(x)$ is expressed in parametric form with respect to the strain e according to (3.21)–(3.23), while the end values of the strain e_0, e_L are calculated by solving the system (3.24), (3.25).

Several features of the above solution merit attention at this point. It is tacitly assumed here that e varies monotonically between e_0 and e_L with $e_0 > e > e_L$. The assumption $e_0 > e_L$ does not impair generality for it simply implies that the highest strain occurs at $x = 0$. The choice $e_L > e_0$ produces the mirror strain distribution about $x = L/2$. The monotonicity of e in the interval $[0, L]$, i.e. $e_{,x} < 0$ for $0 < x < L$, implies from (3.20), (3.22) that

$$W(e) - W(e_0) \geqslant c(e - e_0),$$

or equivalently

$$W(e) - W(e_L) \geqslant c(e - e_L), \tag{3.26}$$

where the equality holds only at $e = e_0$ or $e = e_L$. A direct consequence of (3.26) which follows by taking the limits $e \to e_0$ and $e \to e_L$ is

$$W'(e_0) \leqslant c \leqslant W'(e_L). \tag{3.27}$$

The strain at bifurcation e_1 is the limit of e_0, e_L as the principal solution is approached from the bifurcated equilibrium solution. Recall $e_0 \geqslant e_1 \geqslant e_L$.

The geometrical interpretation of the end force c (constant throughout the structure) and the inequalities (3.26), (3.27) is depicted in the graph of the macroscopic stress $W'(e)$ – strain e relation shown in Fig. 3.1. The force c is

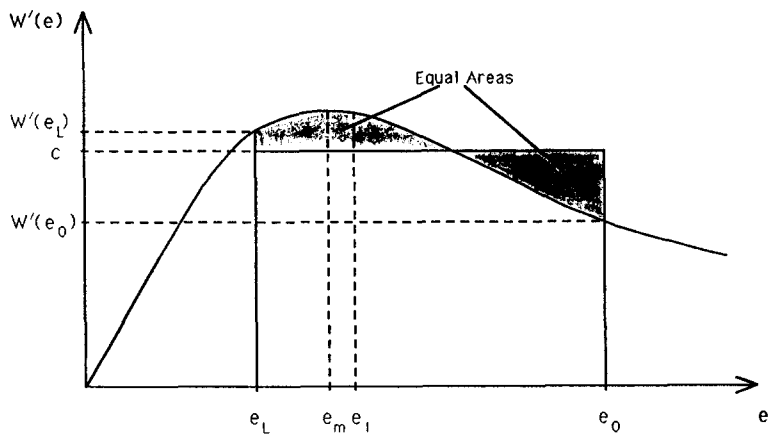

Fig. 3.1. Geometric construction of the end force c acting on a bar with macroscopic stress–strain relation given by $W'(e)$ and the maximum and minimum strains respectively e_0 and e_L.

found by constructing a line parallel to the e axis that cuts equal areas above and below the graph of $W'(e)$ between e_L and e_0. For the curve $W'(e)$ depicted in Fig. 3.1 with a monotonically decreasing branch for $e > e_m$ the inequalities (3.26) and (3.27) may be satisfied for all $e_0 > e_1$.

A typical graph for the strain distribution $e = u_{,x}$ according to (3.21) as a function of x is depicted in Fig. 3.2(a) for $e_0 > e_L$ (and in Fig. 3.2(b) for $e(0) = e_L$, $e(L) = e_0$). The localization of the deformation pattern near $x = 0$ is obvious. The corresponding eigenmode at the bifurcation strain e_1 is also shown for comparison.

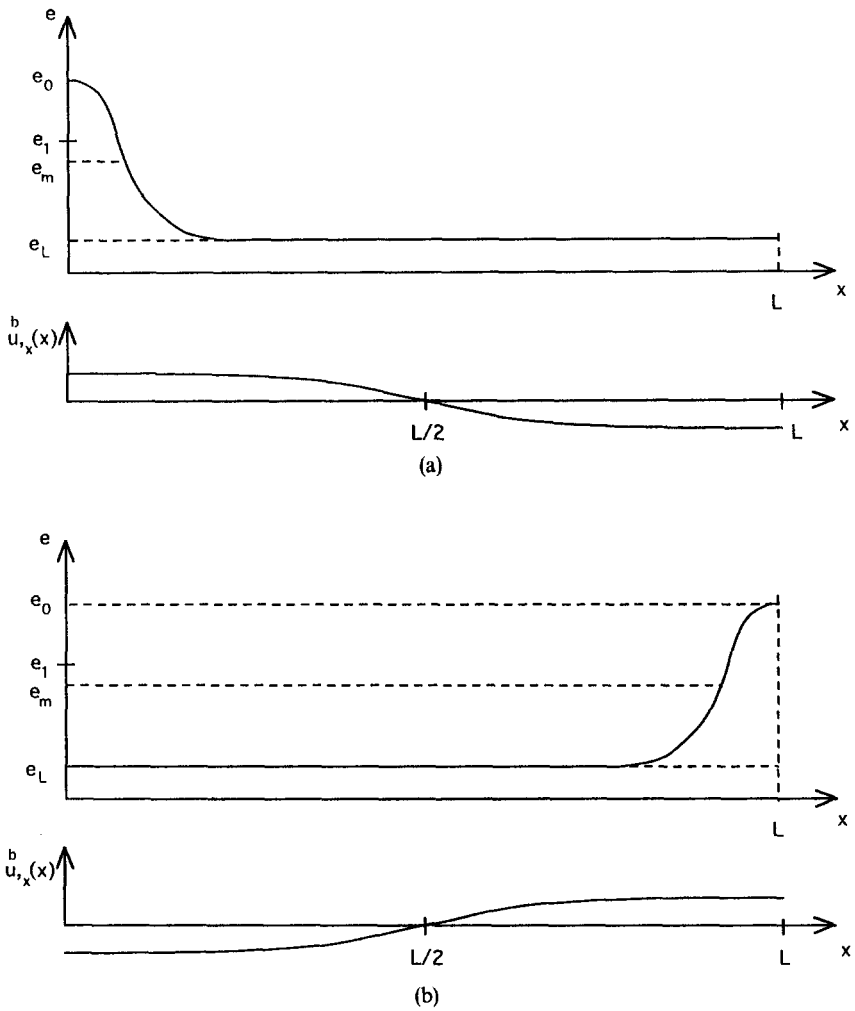

Fig. 3.2. Typical strain profile and corresponding bifurcation eigenmode for bifurcated equilibrium solutions emerging at $\Delta_1 = e_1 L$: (a) when the maximum strain occurs at $x = 0$ and (b) when the maximum strain occurs at $x = L$.

The generalization of the above results to include the bifurcated equilibrium solutions emerging from any other root $e_n = \Delta_n/L$ of (3.15) does not present any difficulties. As suggested by the corresponding strain eigenmode $\cos(n\pi x/L)$, which for $n > 1$ is no longer monotonically varying with x but varies periodically between a maximum and minimum value, the bifurcated equilibrium solution is periodic in $[0, L]$ with semi-period L/n. The strain $e = u_{,x}$ varies between a maximum of e_0 and a minimum of e_L. Within each such half period (3.21)–(3.23) still hold while (3.24) and (3.25) are modified to

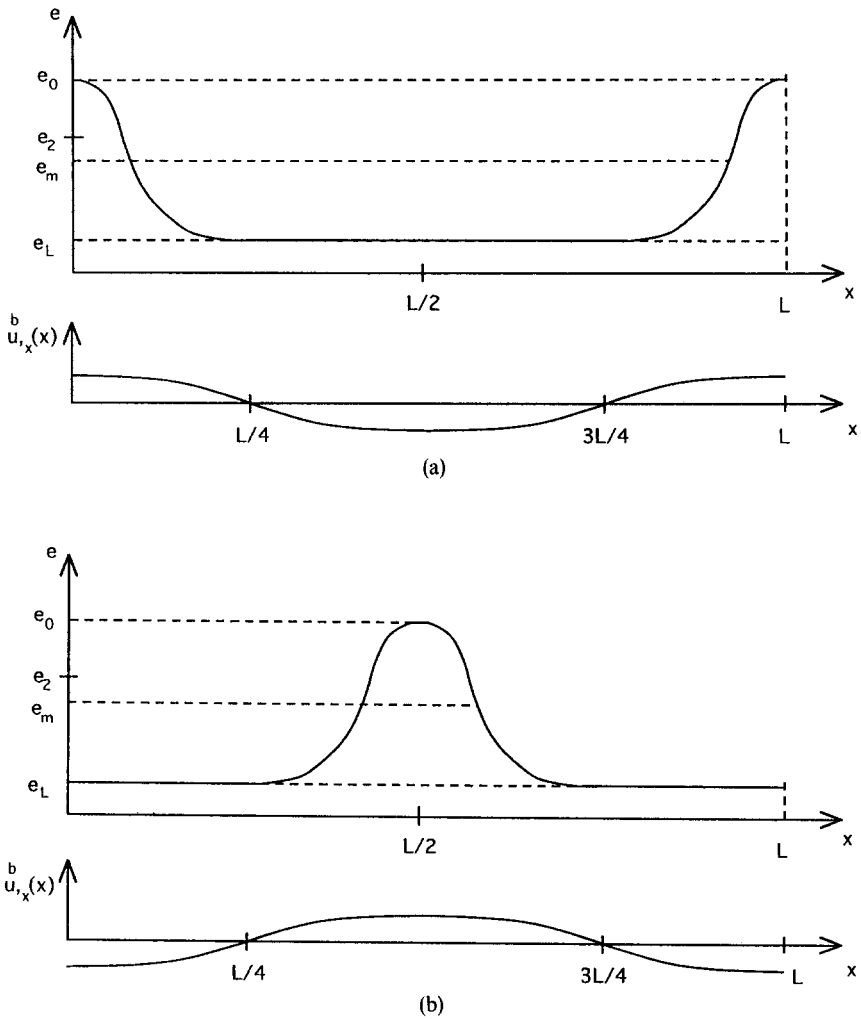

Fig. 3.3. Typical strain profile and corresponding bifurcation eigenmode for bifurcated equilibrium solutions emerging at $\Delta_2 = e_2 L$: (a) when the maximum strain occurs at $x = 0$ and (b) when the maximum strain occurs at $x = L/2$.

read

$$\frac{L}{n} = \varepsilon \int_{e_L}^{e_0} \{h(e)/2[W(e) - W(e_0) - c(e - e_0)]\}^{1/2}\, de, \tag{3.28}$$

$$\frac{\Delta}{n} = \varepsilon \int_{e_L}^{e_0} e\{h(e)/2[W(e) - W(e_0) - c(e - e_0)]\}^{1/2}\, de. \tag{3.29}$$

The bifurcated equilibrium solutions which emerge from Δ_n can be easily constructed by matching the equilibrium solution (3.21)–(3.23) and (3.28),

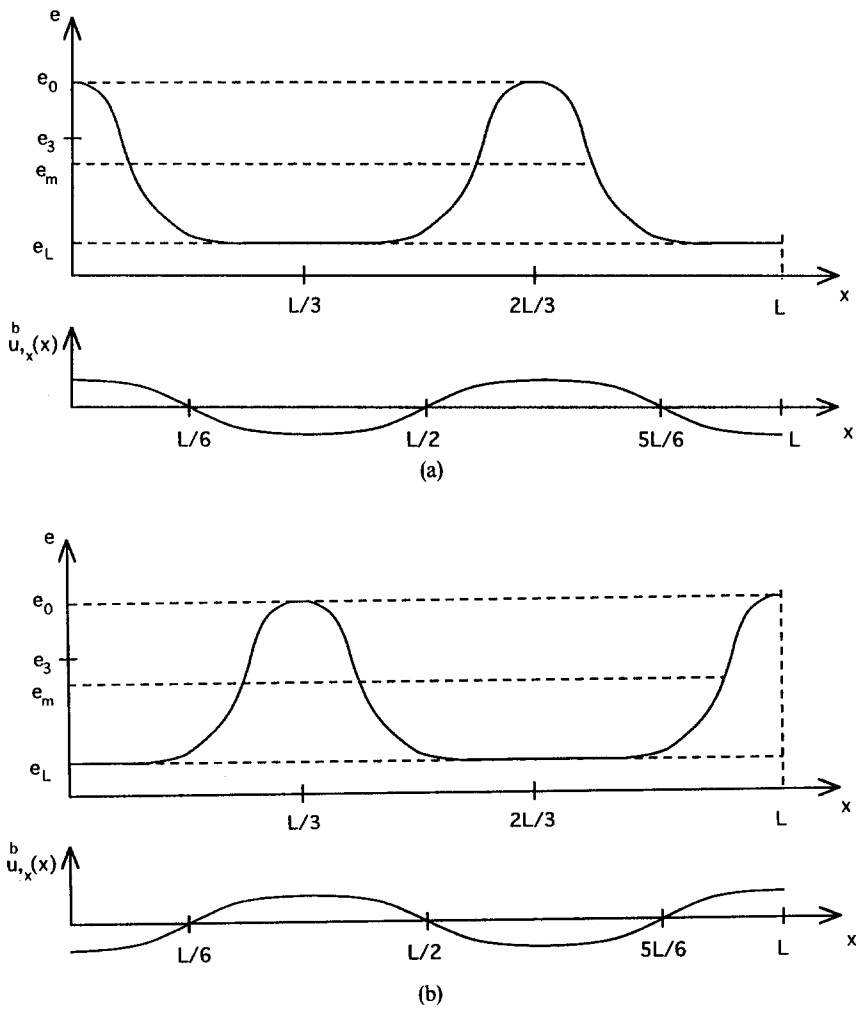

Fig. 3.4. Typical strain profile and corresponding bifurcation eigenmode for bifurcated equilibrium solutions emerging at $\Delta_3 = e_3 L$: (a) when the maximum strain occurs at $x = 0$ and (b) when the maximum strain occurs at $x = L/3$.

(3.29) over the half period L/n and its mirror image (obtained when $e_0 < e_L$) at the points $x = mL/n$ where $m = 1, 2, \ldots, n-1$. The so constructed equilibrium solution $u(x)$ is C^2 continuous in the interval $[0, L]$, i.e. u, $u_{,x}$ $u_{,xx}$ are continuous functions of x on $[0, L]$.

The strain distributions for the bifurcated solutions from Δ_2, Δ_3, Δ_4 together with their corresponding eigenmodes are depicted in Figs. 3.3–3.5. The construction of all other bifurcated solutions (i.e. for $n > 4$) follows easily.

To each bifurcation point Δ_n correspond two bifurcated equilibrium solutions as seen in Figs. 3.2–3.5. Solutions (a) correspond to the maximum strain

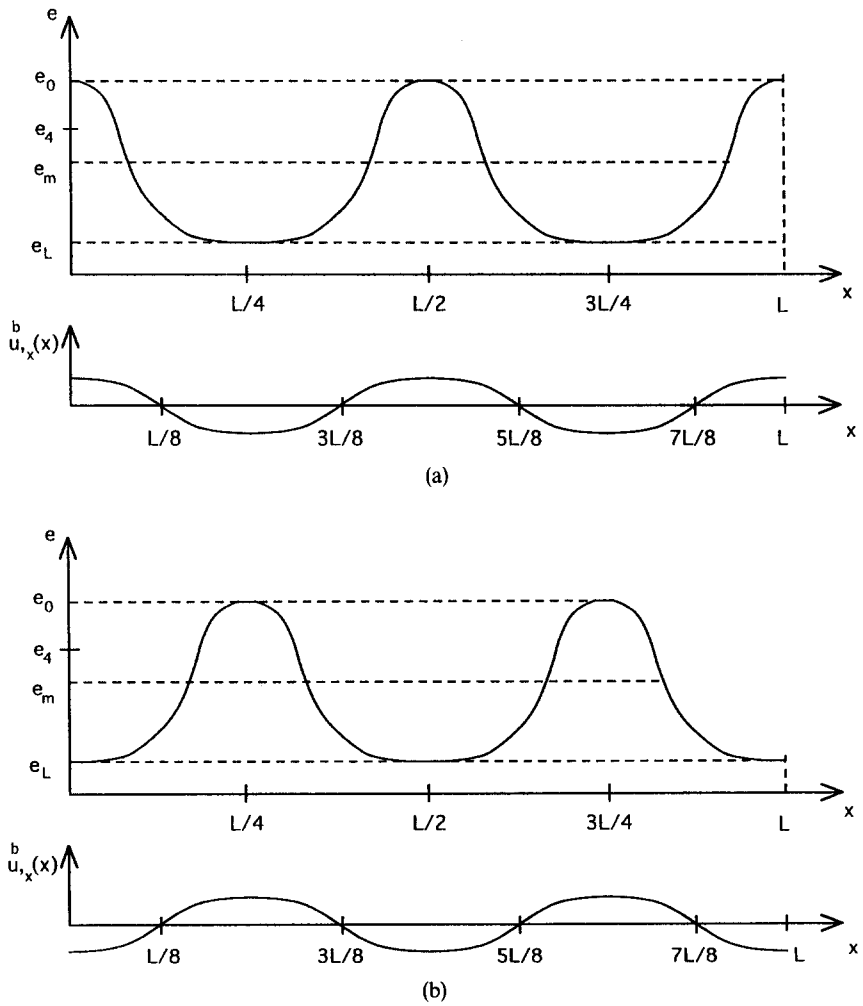

Fig. 3.5. Typical strain profile and corresponding bifurcation eigenmode for bifurcated equilibrium solutions emerging at $\Delta_4 = e_4 L$: (a) when the maximum strain occurs at $x = 0$ and (b) when the maximum strain occurs at $x = L/4$.

e_0 occurring at $x = 0$ while solutions (b) correspond to the minimum strain e_L occurring at $x = 0$. Notice that for odd values of n the (a) and (b) equilibrium solutions are mirror images of each other with respect to $x = L/2$ while for even values of n the (a) and (b) solutions are different.

4. Comparison of solutions for discrete and continuum models

4.1. General remarks

Two different types of models will be investigated in this section, according to their macroscopic behavior, i.e. according to the properties of $W(u_{,x})$ in (3.1). The first model, which will also be subsequently referred to as the type A model, has a stress–strain behavior $W'(e) - e$ ($e = u_{,x}$) that is increasing for $0 \leqslant e < e_m$ and for $e > e_m^* > e_m$ with $W'(e) \to \infty$ as $e \to \infty$, while it decreases for $e_m < e < e_m^*$ as shown in Fig. 4.1(a). Such models are typically employed in calculations involving phase changes in solids as for example in James [19] and modeling dissipative response in elastoplasticity as in Abeyaratne and Knowles [2, 3]. The second model, which will also be subsequently referred to as the type B model, has a stress–strain behavior $W'(e) - e$ that is monotonically increasing for $0 \leqslant e < e_m$ and monotonically decreasing for $e > e_m$ with $W'(e) \to 0$ as $e \to \infty$ as shown in Fig. 4.1(b). Models of this type have been employed in calculations involving progressive loss of load bearing capacity in solids past a certain critical strain and are essentially used in the soils-geomaterials literature often in association with damage as for example in Bažant [10] and Lasry and Belytschko [23].

A common feature of both the type A and type B models investigated here is that they each involve springs of length ε and 2ε, i.e. $q = 2$ (see discussion in Section 2.1). The reason for this choice lies in the requirement (3.11) which mandates $h(u_{,x}) > 0$. Had only springs of length ε been used in the model, i.e. $q = 1$, according to (3.4) $W(u_{,x}) = w_1(u_{,x})$ and $h(u_{,x}) = -w_1''(u_{,x})/12$, which are in obvious contradiction to the requirements (3.10) and (3.11).

The stability investigation of the equilibrium solutions is important, for it determines when a particular equilibrium branch is stable and thus observable in a quasistatic loading experiment. The stability of the principal solution for the continuum model has already been presented in Section 3.4. The stability calculations for all the equilibrium solutions (principal and bifurcated) of the discrete model are done numerically by investigating the positive definiteness of the second derivative of the potential energy $\mathscr{E}_{,uu}$, subject to the displacement constraints $u_0 = 0$, $u_N = \Delta$, evaluated at the equilibrium solution in question. Note that $\mathscr{E}_{,uu}$ is the stiffness matrix required by the incremental Newton-Raphson procedure, whose $[L][D][U] = [\mathscr{E}_{,uu}]$ decomposition ($[L]$ is a

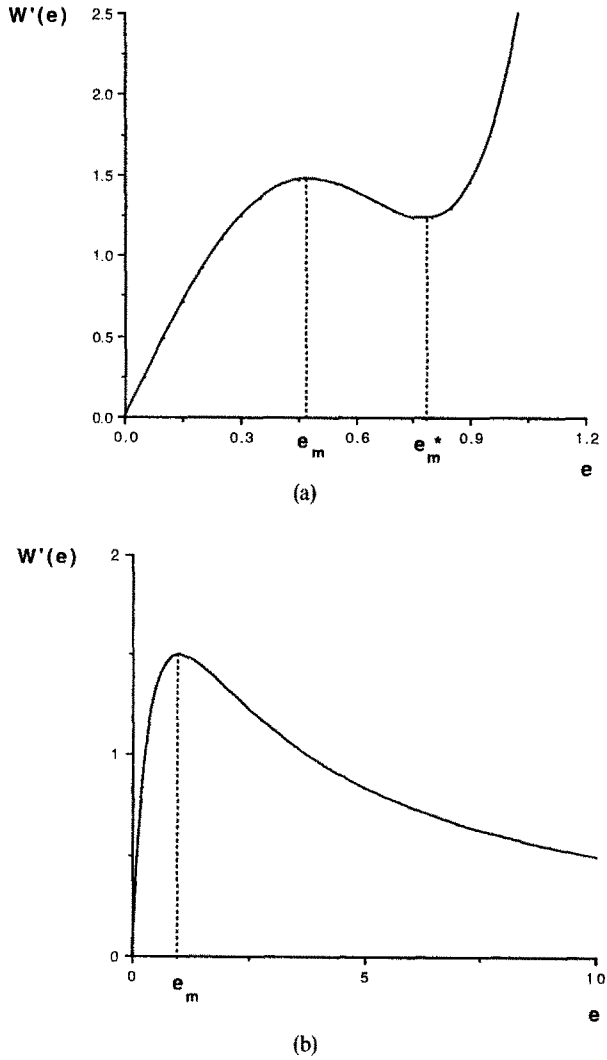

Fig. 4.1. Macroscopic stress–strain behavior (a) for the type A model and (b) for the type B model based on the actual discrete micromodels employed in all the numerical/analytical calculations (see Sections 4.2 and 4.3 for the employed constants respectively).

lower triangular matrix with unit diagonal elements, $[D]$ is a diagonal matrix and $[U] = [L]^T$) is automatically performed at every loading step as part of the solution procedure. Stability is simply decided by the sign of $d \equiv \min_{(i=1,\ldots,N-1)} D_{ii}$ where D_{ii} are the diagonal elements of $[D]$ ($d > 0 \Rightarrow \mathscr{E}_{,uu}$ is positive definite and hence the equilibrium solution under investigation is stable).

The issue of imperfection sensitivity also merits attention. As discussed in Section 3.4, the perfect continuum structure of length L has bifurcation points

at strains $e_n = \Delta_n/L$, and these bifurcations occur just past the strain level e_m corresponding to the maximum stress ($e_m < e_1 < e_2 < \cdots$). As the structure's length increases all bifurcation strains approach e_m. Exactly the same behavior is exhibited by the perfect discrete structure as has been verified numerically for all the examples considered in this work. Given that the occurrence of imperfections is inevitable in practice, the question that naturally arises is which will be the (unique) equilibrium branch followed during a loading history, starting at rest, of the imperfect structure.

The answer to this question is simple. For small imperfections (taken here in the form of slightly different spring properties) the equilibrium solution remains close to the uniform strain solution of the perfect structure as long as all springs have strains lower than e_m. As soon as the weakest spring's strain exceeds e_m a strongly localized deformation solution develops with a strain distribution in the form of Fig. 3.3(b) with the maximum strain occurring at the weakest spring. It has been verified numerically that although the location of the maximum strain depends on the site of the weakest spring, the bell shape of the strain distribution is very close to the bifurcated solution of the perfect structure that emerges from Δ_2 (and whose corresponding eigenmode is $\overset{2}{u}(x) = \cos(2\pi x/L)$). In addition the force F–end displacement Δ curves of these equilibrium solutions, which are essentially different from each other by a translation, are almost identical, as are their elastic energies (for a given strain at the weakest spring).

The above results show that the most interesting, from a practical viewpoint, localized strain equilibrium solution is the full bell-shaped one with strains decaying on either side of the maximum strain. In order to avoid the introduction of imperfections in the model, and in view of the fact that the perfect structure's bifurcated branch emerging from Δ_2 is energetically almost neutral to parallel translations (i.e. for $\delta u(x) = \text{const}$), the stability of this bifurcated equilibrium solution is studied under the additional assumption of the prescribed displacement $u(L/2) = \Delta/2$. This additional kinematic requirement plays the role of an imperfection at $L/2$, thus pinning the maximum strain at this point and stabilizing the solution against parallel translations. It should be mentioned at this point that an analytical investigation of the stability of the equilibrium solutions in a perfect infinite solid with continuum energy density given by (3.1) was presented by Alexiades and Aifantis [8] while Carr, Gurtin and Slemrod [11] discussed the corresponding finite dimensional case. Their results are in agreement with the present investigation's findings that only the solutions with monotonically varying strain are stable (assuming no intermediate constraints of course).

Three sets of graphs will be presented for each model type, comparing the results for the discrete and continuum version of each model. The first set of graphs will display the end load F–end displacement Δ curves for the principal

and bifurcated equilibrium solutions. For the continuum model the end force $F = c$ where $c = W'(\overset{0}{e})$ for the principal solution and $c = (W(e_0) - W(e_L))/(e_0 - e_L)$ for the bifurcated solutions (see (3.7), (3.22)). For the discrete model $F = \Sigma_{p=1}^{q} \Sigma_{r=1}^{p} f_p(e_p^{(N-r)^+})$.

The second set of graphs will display bifurcated (localized strain) solution strain distributions for the discrete and continuum versions of each model. All comparisons presented are taken from stable (and thus observable) parts of the bifurcated branches.

The third set of graphs will display the stability results for the bifurcated equilibrium solutions of interest. In view of the close agreement between the continuum and discrete models, only the discrete model's stability calculations are presented.

4.2. Type A model

For this model, whose macroscopic stress $W'(e)$ – strain e behavior has two increasing branches for $0 \leqslant e < e_m$ and $e_m^* < e < \infty$ and a decreasing one for $e_m < e < e_m^*$, the energies $w_1(e)$ and $w_2(e)$ are the following sixth order polynomials

$$w_i(e) = \frac{1}{2} K_i e^2 - \frac{1}{4} M_i e^4 + \frac{1}{6} N_i e^6, \quad i = 1, 2, \quad e \equiv u_{,x}. \tag{4.1}$$

According to (3.4) the corresponding continuum energy density has the following form for $W(e)$ and $h(e)$ where $e \equiv u_{,x}$:

$$W(e) = \frac{1}{2}(K_1 + 2K_2)e^2 - \frac{1}{4}(M_1 + 2M_2)e^4 + \frac{1}{6}(N_1 + 2N_2)e^6, \tag{4.2}$$

$$h(e) = -\frac{1}{12}(K_1 + 8K_2) + \frac{3}{12}(M_1 + 8M_2)e^2 - \frac{5}{12}(N_1 + 8N_2)e^4. \tag{4.3}$$

The monotonicity of $W'(e)$ for e near zero and also for large values of e dictates that $(K_1 + 2K_2) > 0$ (I.1) and $(N_1 + 2N_2) > 0$ (I.2). The strains e_m and e_m^* corresponding to the maximum and minimum stresses respectively, are

$$\begin{aligned} e_m &= \left[\frac{3(M_1+2M_2) - [9(M_1+2M_2)^2 - 20(K_1+2K_2)(N_1+2N_2)]^{1/2}}{10(N_1+2N_2)}\right]^{1/2} \\ e_m^* &= \left[\frac{3(M_1+2M_2) + [9(M_1+2M_2)^2 - 20(K_1+2K_2)(N_1+2N_2)]^{1/2}}{10(N_1+2N_2)}\right]^{1/2} \end{aligned} \tag{4.4}$$

For the above values of e_m, e_m^* to be real, it is tacitly assumed that

$3(M_1+2M_2) > [20(K_1+2K_2)(N_1+2N_2)]^{1/2}$ (I.3). In addition the requirement (3.11) that $h(e) > 0$ dictates from (4.3) that $(K_1+8K_2) < 0$ (I.4), $(M_1+8M_2) > 0$ (I.5), $(N_1+8N_2) < 0$ (I.6). The constants used in this model are

$$K_1 = 10, \qquad M_1 = 10, \qquad N_1 = 20,$$
$$K_2 = -2.5, \qquad M_2 = 0, \qquad N_2 = -6.4.$$

which satisfy the above-mentioned inequalities (I.1)–(I.6). According to $(4.4)_1$, the local maximum stress of the principal solution (discrete and continuum) occurs at $e_m = 0.47992$. The corresponding macroscopic stress $W'(e)$ – strain e diagram is depicted in Fig. 4.1(a).

The lengths $L = 96\varepsilon$ and $\varepsilon = 1$ are used in all subsequent calculations.

4.2.1. Comparison of end force–end displacement diagrams

The end force F –(dimensionless) end displacement Δ/L diagrams which show the equilibrium paths of the type A discrete and continuum models are depicted in Fig. 4.2(a), (b).

The first four bifurcation points $e_n = \Delta_n/L$ ($n = 1, 2, 3, 4$) for the continuum and the discrete models are listed below.

Continuum	Discrete
$e_1 = 0.480099$	$e_1 = 0.480099$
$e_2 = 0.480626$	$e_2 = 0.480625$
$e_3 = 0.481509$	$e_3 = 0.481505$
$e_4 = 0.482761$	$e_4 = 0.482724$

Recall that the bifurcation points for the continuum model are the appropriate roots of (3.15), where $W(e)$ and $h(e)$ are given by (4.2), (4.3). The corresponding bifurcation points for the discrete model are found by investigating the positive definiteness of the stability matrix $\mathscr{E}_{,uu}(\overset{0}{u}, \Delta)$ subject to the constraints $\delta u(0) = \delta u(L) = 0$ for the first bifurcation point $e_1 = \Delta_1/L$, $\delta u(0) = \delta u(L/2) = \delta u(L) = 0$ for $e_2 = \Delta_2/L$, $\delta u(0) = \delta u(L/3) = \delta u(2L/3) = \delta u(L) = 0$ for $e_3 = \Delta_3/L$ and so on, since the corresponding eigenmode must vanish at these intermediate nodes. As expected, the accuracy of the continuum model decreases for higher eigenmodes, but it is quite remarkable that for the modes investigated the disagreement does not exceed 0.008%. Similarly, remarkably good agreement is found for the bifurcated (localized strain) equilibrium solutions.

Certain important features of the bifurcated equilibrium solutions depicted in Fig. 4.2 are worth discussing. The first such feature is that bifurcation

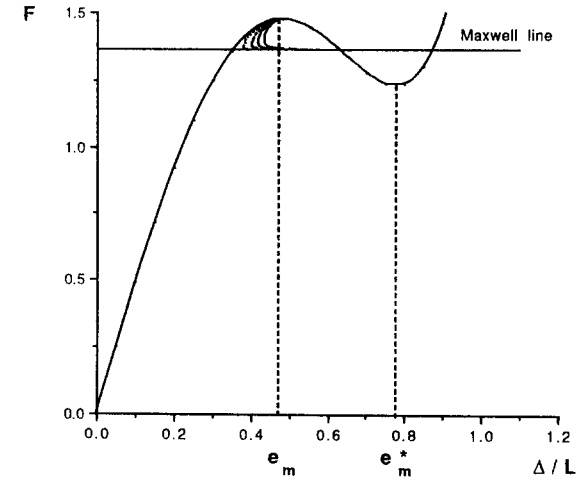

(a)

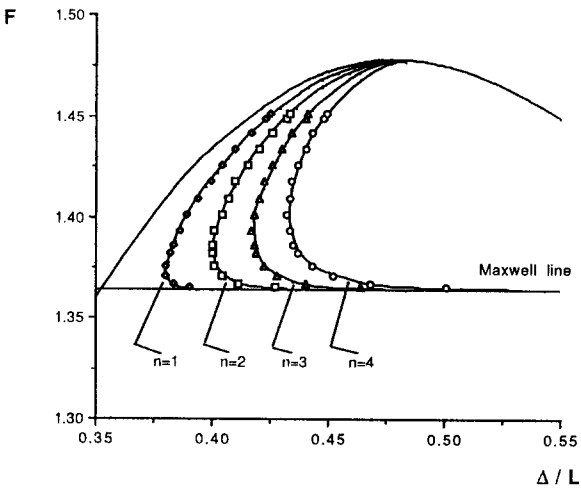

(b)

Fig. 4.2. Comparison of the end force F–(dimensionless) end displacement Δ/L for a type A model of length $L = 96\varepsilon$ based on the continuum (solid line) and discrete (point marks) solutions for the first four ($n = 1, 2, 3, 4$) bifurcated solutions. Fig. 4.2(b) is an enlarged version of Fig. 4.2(a).

initially occurs at decreasing end displacement. Indeed at localization one or a few springs experience an increase in strain to a value above the critical strain, while the majority of springs experience a reduction in strain to a value below the critical strain in order to satisfy the equilibrium equation for the structure. This reduction in strain in the majority of springs is responsible for the overall decrease of the end displacement Δ from its critical value.

As a bifurcation amplitude parameter that increases monotonically in the

bifurcated equilibrium branch, we consider the maximum strain e_0 (see Section 3.4.2). As the maximum strain e_0 increases, one can see from the graphic construction in Fig. 3.1 that the minimum strain e_L decreases. For a type A material, the minimum value of e_L that can be achieved without violating (3.26), (3.27) is the lower strain $\hat{e}_L$, while the peak strain at the localized zone approaches $\hat{e}_0$, where $\hat{e}_L$, $\hat{e}_0$ are the strains for which the force $\hat{c} = (w(\hat{e}_0) - w(\hat{e}_L))/(\hat{e}_0 - \hat{e}_L)$ (see equation (3.22)) is the Maxwell line of the stress $W'(e)$ – strain e curve ($\hat{c} = W'(\hat{e}_L) = W'(\hat{e}_0)$). See Fig. 4.3.

Since in the bifurcated solution the force c should exceed $\hat{c}$ (according to (3.26), (3.27)), it follows that all the bifurcated equilibrium solutions lie above the Maxwell line, exactly as seen in Fig. 4.2.

The evolution of each bifurcated equilibrium solution proceeds as follows. As the peak strain e_0 increases away from the bifurcation strain, the strain within the localized deformation zone increases while its size decreases rapidly from L/n to a fraction of L/n, attaining its minimum value. Thereafter the localized deformation zone size begins to slowly increase. As e_0 approaches $\hat{e}_0$, the localized deformation zone increases rapidly in size, and spreads across the entire length of the structure. Subsequently, a uniform strain solution develops with $e > \hat{e}_0$ throughout the structure. The above behavior of the onset and propagation of the localized deformation zone is similar to the one reported in Kyriakides and Chang [22] who study the propagation of a bulge in an inflatable elastic cylindrical member subjected to internal pressure, although their model is an axisymmetric (two-dimensional) nonlinear elastic membrane

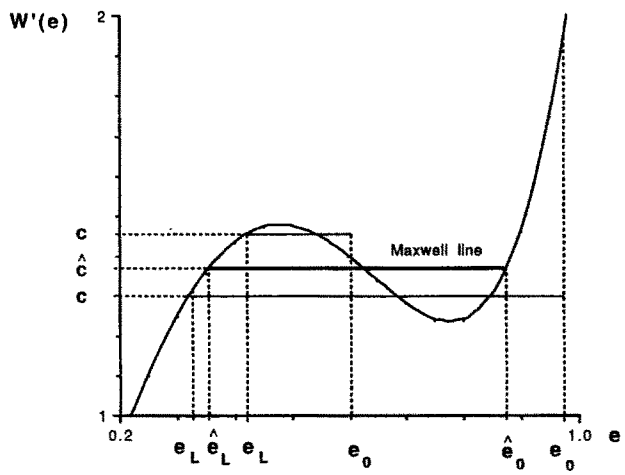

Fig. 4.3. Graphic interpretation of the admissibility of solutions with maximum strain $e_0 < \hat{e}_0$ and inadmissibility of solutions with $e_0 > \hat{e}_0$ for continuum models of type A, where $\hat{e}_0$ and $\hat{e}_L$ are the maximum and minimum strains corresponding to the Maxwell line.

model as opposed to the one-dimensional higher order gradient model employed here.

The most interesting feature in the continuum bifurcated equilibrium solutions shown in Fig. 4.2 is that they stop as $\Delta/L \to \hat{e}_0$. This is a limitation of the analytical model considered in (3.1), (3.7). For as long as the maximum strain $e_0 < \hat{e}_0$, a constant c can be found from (3.22) that satisfies the inequalities (3.26), (3.27). Any solution with $e_0 > \hat{e}_0$ violates (3.27) as one can see graphically from Fig. 4.3. The discrete solution does not suffer any such limitation. Notice the excellent agreement between the discrete and continuum bifurcated solutions at the initial part of the formation of the localized strain zone for $n = 1, 2, 3, 4$, as seen in Fig. 4.2(b).

4.2.2. Comparison of strain profiles

In addition to the comparison of the force F–(dimensionless) end displacement Δ/L diagrams, the strain profiles of the localized equilibrium solutions are compared in Fig. 4.4(a), (b), (c). The above strain distributions correspond to the first bifurcated solution of a structure of length $L = 96\varepsilon$ subject to $u(L/2) = \Delta/2$ or equivalently, as discussed in Section 4.1, to the second bifurcation of the same structure without the above constraint. (The solution also coincides with the first bifurcated solution of a structure with $L = 48\varepsilon$.) This equilibrium solution has a bell-shaped strain profile symmetric about $x = L/2$ as discussed in Section 3.4.2 (see Fig. 3.3(b)) and thus only the right half is partially shown in Fig. 4.4. For the discrete model the strains in the springs of length ε, $e_1^{i-} = (u_i - u_{i-1})/\varepsilon$, are plotted against node numbers i (for $i > N/2 = 48$). For the continuum model the corresponding quantities are the average strains between nodes i and $i-1$, $\bar{e}_i = (1/\varepsilon)\int_{(i-1)\varepsilon}^{i\varepsilon} e\,dx = u(i) - u(i-1)$ (recall $\varepsilon = 1$), and are plotted for the same range of node numbers.

The above strain distributions have been calculated for force levels $c_a = 1.377$, (a) $c_b = 1.369$, (b) and $c_c = 1.365$, (c) all of which are stable, and therefore observable, points along the bifurcated equilibrium path. Notice the excellent agreement between the discrete and continuum model strain distributions at load points away from the Maxwell line load ($\hat{c} = 1.364$), Fig. 4.4(a), (b). As the Maxwell line is approached and the localized strain zone begins to propagate through the model, the discrepancies between the discrete and continuum strain profiles become noticeable, Fig. 4.4(c), in view of the limitations of the continuum model in describing the propagation phase of the localized deformation.

4.2.3. Discussion of stability

Finally our attention is turned to the discussion of stability for the bifurcated equilibrium solutions. For the reasons explained in Section 4.1, we investigate

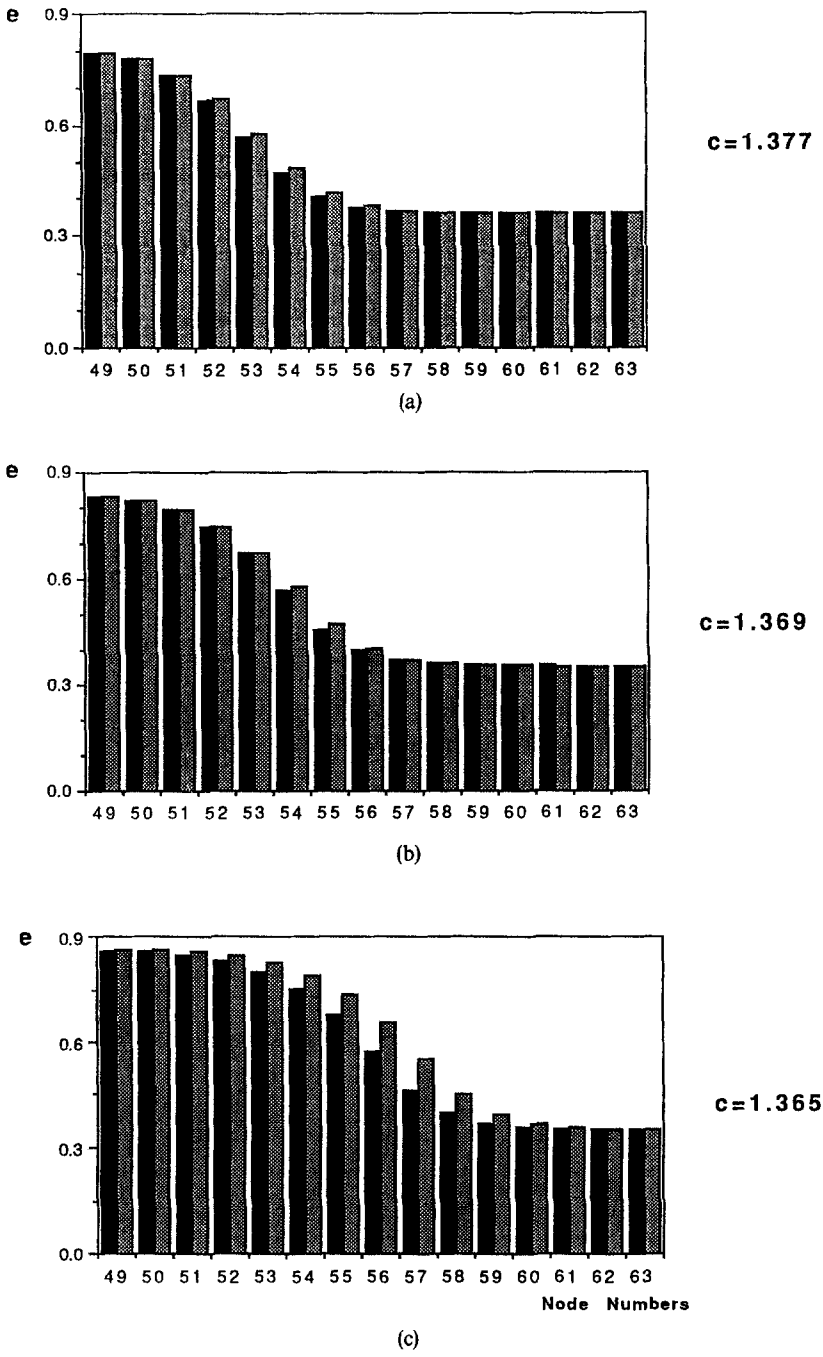

Fig. 4.4. Comparison of strain profiles of discrete (solid bars) and continuum (shaded bars) solutions at three different load levels for the type A model with length $L = 96\varepsilon$. All comparisons are within the stable range of the bifurcated equilibrium branch emerging from $\Delta_2 = e_2 L$. Only the right halves of the "bell-shaped" localized strain solutions are partially depicted here.

the stability of the symmetric bifurcated equilibrium solution with the localized strain zone centered at $x = L/2$ (the bifurcated equilibrium path emerging from Δ_2), subject to $u(L/2) = \Delta/2$. For comparison the stability of the asymmetric bifurcated equilibrium solution with the localized strain zone centered at $x = 0$ (or $x = L$), i.e. the bifurcated equilibrium path emerging from Δ_1, is also presented. The results are depicted in Fig. 4.5. Solid lines represent stable equilibrium configurations while dashed lines represent unstable ones.

Notice that the localized deformation solutions change stability at the point where the end displacement Δ stops decreasing, i.e. at $dF/d\Delta = \infty$. The mechanism which stops the decrease in end displacement and causes the end displacement to increase is both the growth of the maximum strain e_0, and the growth of the localized strain zone size. The importance of these stability results lies in the fact that they show stability of the localized strain solutions after a minimum value of the applied displacement has been reached (at $dF/d\Delta = \infty$) during the localization process. Stability of the localized deformation branch means observability in a quasistatic loading experiment. The stability results presented here are based on the discrete model.

4.3. Type B model

For this model, whose macroscopic stress $W'(e)$ – strain e behavior increases monotonically to a maximum stress at e_m and then monotonically decreases to zero stress as $e \to \infty$, the energies $w_1(e)$ and $w_2(e)$ respectively, are

$$\left.\begin{aligned} w_1(e) &= -7 + e + 6\ln(1+e) + \frac{7}{1+e} \\ w_2(e) &= -\frac{1}{2}\left(-1 + e + \frac{1}{1+e}\right) \end{aligned}\right\} e \equiv u_{,x}. \tag{4.5}$$

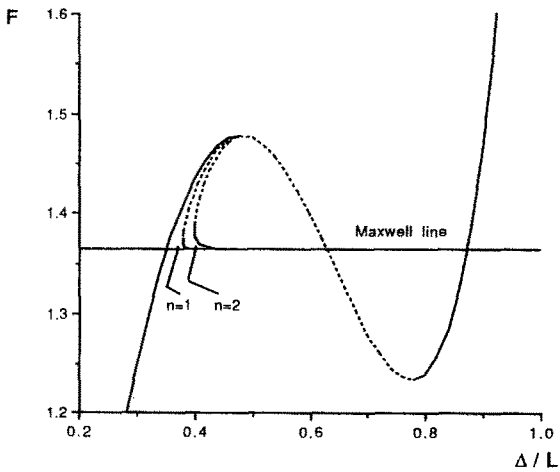

Fig. 4.5. Stable (solid line) and unstable (dashed line) regions of the principal and the first two ($n = 1, 2$) bifurcated equilibrium paths for the type A model of length $L = 96\varepsilon$.

According to (3.4) the corresponding continuum energy density has the following form for $W(e)$ and $h(e)$

$$W(e) = 6\left[\ln(1+e) - \frac{e}{1+e}\right], \tag{4.6}$$

$$h(e) = \frac{1}{2}\frac{e}{(1+e)^3}. \tag{4.7}$$

Attention is restricted here to tensile deformation $e > 0$.

The requirement (3.11) that $h(e) > 0$ is automatically satisfied. Moreover (3.10) also holds and the maximum stress in the principal solution occurs for

$$e_m = 1. \tag{4.8}$$

The corresponding macroscopic stress $W'(e)$ – strain e diagram is depicted in Fig. 4.1(b).

As for the type A models, the lengths $L = 96\varepsilon$ and $\varepsilon = 1$ are used in all subsequent calculations.

4.3.1. Comparison of end force – end displacement diagrams

The end force F – (dimensionless) end displacement Δ/L diagrams which show the equilibrium paths of the type B discrete and continuum models are depicted in Fig. 4.6(a), (b).

The first four bifurcation points $e_n = \Delta_n/L$ ($n = 1, 2, 3, 4$) for the continuum and the discrete model are listed below.

Continuum	Discrete
$e_1 = 1.000089$	$e_1 = 1.000089$
$e_2 = 1.000357$	$e_2 = 1.000357$
$e_3 = 1.000804$	$e_3 = 1.000802$
$e_4 = 1.001430$	$e_4 = 1.001412$

The procedures used to obtain the above results for the continuum and discrete models are identical to the ones followed for the type A model. The accuracy of the continuum models is even more remarkable since the maximum discrepancy, which is observed for the fourth eigenvalue, is 0.0016%.

For the same reasons given for the type A model, each bifurcated equilibrium solution occurs initially at decreasing end displacement Δ.

Again the monotonically increasing parameter along the bifurcated equilibrium branch is the maximum strain e_0. Unlike the previous model, there is

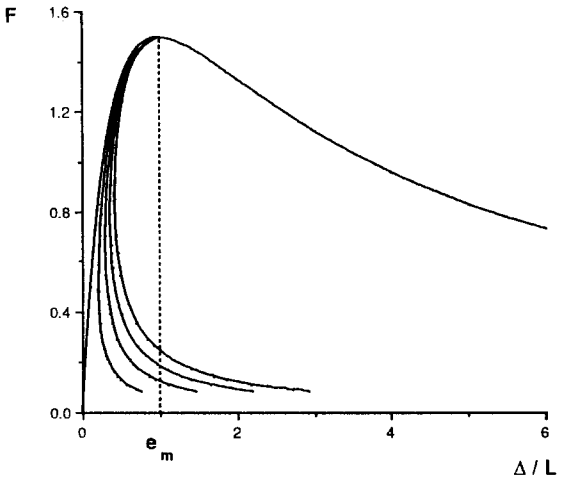

(a)

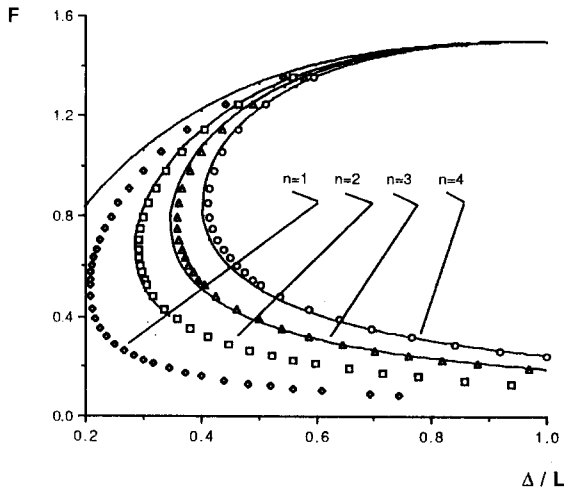

(b)

Fig. 4.6. Comparison of the end force F – (dimensionless) end displacement Δ/L for the type B model of length $L = 96\varepsilon$ based on the continuum (solid line) and discrete (point marks) solutions for the first four ($n = 1, 2, 3, 4$) bifurcated solutions. Fig. 4.6(b) is an enlarged version of Fig. 4.6(a).

always the possibility of an analytical solution of the continuum model for any level of maximum strain e_0. According to the graphic construction of the force c in Fig. 3.1, one can always find e_L such that the inequalities (3.26), (3.27) are satisfied.

The evolution of the bifurcated equilibrium solution proceeds as follows. As the peak strain e_0 increases away from the bifurcation strain, the strain within the localized deformation zone increases while its size decreases rapidly from

L/n to a fraction of L/n, attaining its minimum value. Thereafter the localized zone size increases very slowly while the peak strain e_0 grows without bound. No propagation is observed. A similar behavior for an infinite medium was found in Triantafyllidis and Aifantis [34].

Notice that the force–displacement diagram of the continuum model is in very good agreement with the results of the discrete model for $n = 2, 3, 4$. For $n = 1$ no analytical solution was calculated due to numerical accuracy limits of the hardware.

4.3.2. Comparison of strain profiles

In addition to the comparison of the force F–(dimensionless) end displacement Δ/L diagrams, the strain profiles of the localized equilibrium solutions are compared in Fig. 4.7(a), (b), (c). The above strain distributions correspond to the first bifurcated solution of a structure of length $L = 96\varepsilon$ subject to $u(L/2) = \Delta/2$ (same conditions as the ones mentioned in Section 4.2.2). Again this equilibrium solution has a bell-shaped strain profile symmetric about $x = L/2$ (see Section 3.4.2; see Fig. 3.3(b)) and thus only the right half is partially shown in Fig. 4.7. The discrete model length ε spring strains are compared to the continuum model average strains between nodes for node numbers $i > 48$. (See Section 4.2.2 for details concerning the construction of the diagrams.)

The above strain distributions have been calculated for force levels $c_a = 0.667$, (a) $c_b = 0.590$, (b) and $c_c = 0.506$, (c) all of which are stable equilibrium configurations. The agreement between the discrete and continuum model strain distributions is good.

4.3.3. Discussion of stability

Finally our attention is turned to the discussion of stability for the bifurcated equilibrium solutions. For the reasons explained in Section 4.1, we investigate the stability of the symmetric bifurcated equilibrium solution with the localized strain zone centered at $x = L/2$ (the bifurcated equilibrium path emerging from Δ_2), subject to $u(L/2) = \Delta/2$. For comparison the stability of the asymmetric bifurcated equilibrium solution with the localized strain zone centered at $x = 0$ (or $x = L$), i.e. the bifurcated equilibrium path emerging from Δ_1, is also presented. The results are depicted in Fig. 4.8. Solid lines represent stable equilibrium configurations while dashed lines represent unstable ones.

As for the type A models, the localized deformation solutions change stability at the point where the end displacement Δ stops decreasing, i.e. at $dF/d\Delta = \infty$. The mechanism which stops the decrease in end displacement and causes the end displacement to increase is the growth without bound of the maximum strain e_0, and the slow growth of the localized strain zone size. As for the type A models the localized strain solutions are stable after a minimum

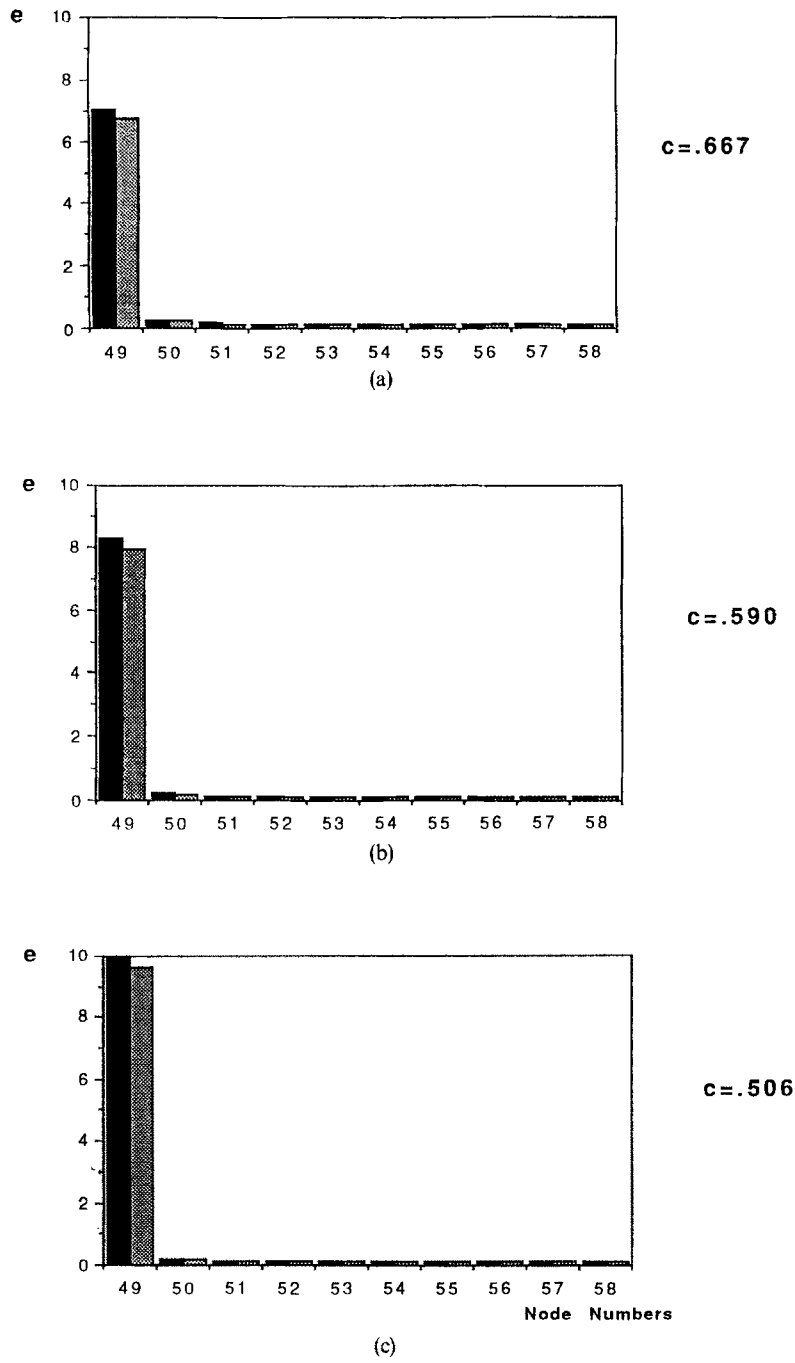

Fig. 4.7. Comparison of strain profiles of discrete (solid bars) and continuum (shaded bars) solutions at three different load levels for the type B model with length $L = 96\varepsilon$. All comparisons are within the stable range of the bifurcated equilibrium branch emerging from $\Delta_2 = e_2 L$. Only the right halves of the "bell-shaped" localized strain solutions are partially depicted here.

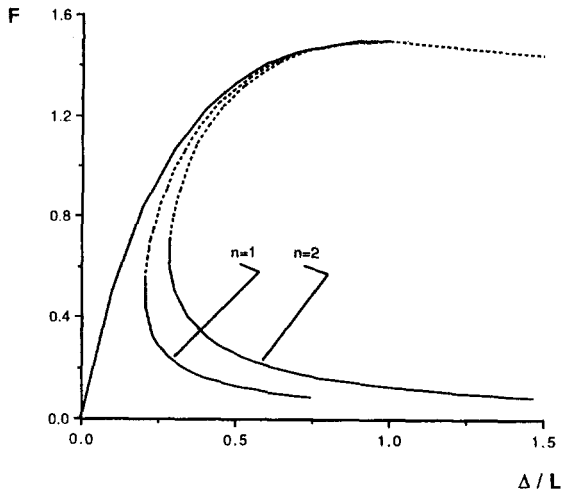

Fig. 4.8. Stable (solid line) and unstable (dashed line) regions of the principal and the first two ($n = 1, 2$) bifurcated equilibrium paths for the type B model of length $L = 96\varepsilon$.

value of the applied displacement is reached during the localization process, and thus are observable in a quasistatic loading experiment.

5. Discussion and concluding remarks

The present study provides a consistent methodology for deriving higher order gradient continuum macroscopic models from the properties of discrete, periodic microstructures. The work is done in the context of one-dimensional nonlinear elastic media, but the methodology can be generalized to planar and space models, as will be shown in a forthcoming paper. Moreover, the accuracy of the continuum models is evaluated via examples where the boundary value problem of stretching a finite length bar is solved twice, once using the discrete model, considered the exact model, and once using the corresponding continuum model, considered the approximate one. It is found that the continuum models that incorporate only up to the second order displacement gradient give very accurate predictions of the end force–end displacement behavior as well as the shape of the localized deformation zone from the onset of localization up to the full development of the zone. For materials that exhibit a local maximum and a subsequent local minimum in their macroscopic stress–strain behavior (referred to in the text as type A materials), the continuum model fails to describe the propagation of the localized deformation zone. Whether the even higher order gradient continuum models – which are easily produced by the proposed method but do not have an analytical

solution – can correct this shortcoming remains to be investigated. This deficiency is absent in materials whose macroscopic stress – strain curves decay to zero stress after reaching a maximum stress (referred to in the text as type B materials), since the maximum strain in the localization zone grows without bound and there is virtually no propagation stage.

The issues of stability and imperfection sensitivity of the localized strain solutions – which are bifurcated solutions away from the uniform strain solution of the bar, occurring slightly after the maximum force is reached – have also been investigated. Of interest are the localized strain equilibrium solutions with a "bell-shaped" strain profile. The reason for our attention to these particular bifurcated solutions lies in the problem's sensitivity to imperfections. It is found that a "bell-shaped" localized strain solution always appears at the weakest point of the structure, irrespective of the exact shape of the imperfection. In addition, the imperfect structure's end force – end displacement and the corresponding strain profiles are essentially the same as the ones of the "bell-shaped" bifurcated solution of the perfect structure. Moreover these solutions are stable once the corresponding end displacement starts increasing (after an initial snap back). Stability implies observability of the "bell-shaped" localized strain equilibrium solutions in a quasistatic loading experiment and thus physical relevance.

The present study is part of a number of recent studies on the relations between the microscopic failure mechanisms and their corresponding macroscopic manifestations in solids with microstructure. In the interest of simplicity as well as mathematical consistency – disordered microstructures present substantial mathematical difficulties once nonlinear phenomena are modeled and require a number of intuitive assumptions which are often difficult to prove – efforts are focused on periodic microstructures and mechanical failure modes during a quasistatic loading process in absence of rate, inertial or thermal effects. Although these studies are more fundamental in nature, they are hoped to lead to better understanding through more accurate modeling of a simple, yet quite useful, class of composites, namely those with periodic (or almost) microstructures, such as certain foam type materials, honeycombs etc. One part of these studies aims at relating macro and micro instability mechanisms at the onset of failure (see Abeyaratne and Triantafyllidis [1], Triantafyllidis and Maker [33], Geymonant, Müller and Triantafyllidis [16]) where the failure mechanism at the micro level is bifurcation buckling and the corresponding failure at the macro level is shear band localization. The present work is the first similar effort in the post failure range, where an effort is made to find continuum theories that are capable of describing the composite's behavior after the onset of the initial instability. Results from the one-dimensional model are very encouraging but more work is needed in studying the problem in two and three dimensions, an investigation that is currently under way.

Acknowledgements

This work was partially funded by ALCOA. The authors are grateful to Dr. Owen Richmond for stimulating discussions and his constant encouragement.

References

1. R. Abeyaratne and N. Triantafyllidis, An investigation of localization in a porous elastic material using homogenization theory. *J. Appl. Mech.* 51 (1984) 481–486.
2. R. Abeyaratne and J.K. Knowles, Non-elliptic elastic materials and the modeling of elastic-plastic behavior for finite deformation. *J. Mech. Phys. Solids* 35 (1987) 343–365.
3. R. Abeyaratne and J.K. Knowels, On the dissipative response due to discontinuous strains in bars of unstable elastic material. *Int. J. Solids Structures* 24 (1988) 1021–1044.
4. E.C. Aifantis and J.B. Serrin, The mechanical theory of fluid interfaces and Maxwell's rule. *J. Coll. and Interf. Sci.* 96 (1983) 517–529.
5. E.C. Aifantis and J.B. Serrin, Equilibrium solutions in the mechanical theory of fluid microstructures. *J. Coll. and Interf. Sci.* 96 (1983) 530–547.
6. E.C. Aifantis, On the microstructural origin of certain inelastic models. Transactions of ASME, *J. Engng. Mat. Tech.* 106 (1984) 326–330.
7. E.C. Aifantis, The physics of plastic deformation. *Int. J. Plasticity* 3 (1987) 211–247.
8. V. Alexiades and E.C. Aifantis, On the thermodynamic theory of fluid interfaces: infinite intervals, equilibrium solutions, and minimizers. *J. Coll. Interf. Sci.* 111 (1986) 119–132.
9. A. Askar, *Lattice Dynamical Foundations of Continuum Theories.* (1985) World Scientific, Singapore.
10. Z.P. Bažant, Softening instability: Part I–Localization into a planar band. *J. Appl. Mech.* 55 (1988) 517–522.
11. J. Carr, M. Gurtin and M. Slemrod, Structured phase transitions on a finite interval. *Arch. Rat. Mech. Anal.* 86 (1984) 317–351.
12. R.J. Clifton, High strain rate behavior of metals. *Appl. Mech. Rev.* 43 (1990) S9–S22.
13. B.D. Coleman, Necking and drawing in polymeric fibers under tension. *Arch. Rat. Mech. Anal.* 83 (1983) 115–137.
14. B.D. Coleman and M.L. Hodgdon, On shear bands in ductile materials. *Arch. Rat. Mech. Anal.* 90 (1985) 219–247.
15. A.C. Eringen and E.S. Suhubi, Nonlinear theory of simple micro-elastic solids–I. *Int. J. Engng. Sci.* 2 (1964) 189–203.
16. G. Geymonant, S. Müller and N. Triantafyllidis, Quelques remarques sur l'homogénéisation des matériaux élastiques nonlinéaires. *C.R. Acad. Sci. Paris*, 311 (Ser. I) (1990) 911–916.
17. J. Hadamard, *Lecons sur la Propagation des Ondes et les Equations de l'Hydrodynamique.* Paris: Hermann (1903) Chap. 6.
18. R. Hill, Acceleration waves in solids. *J. Mech. Phys. Solids* 10 (1962) 1–16.
19. R.D. James, Displacive phase transformations in solids. *J. Mech. Phys. Solids* 34 (1986) 359–394.
20. J.K. Knowles and E. Sternberg, On the failure of ellipticity of the equations for finite elastostatics plane strain. *Arch. Rat. Mech. Anal.* 63 (1977) 321–336.
21. I.A. Kunin, *Elastic Media with Microstructure–I (One-Dimensional Models)* Springer (1982).
22. S. Kyriakides and Y.-C. Chang, The initiation and propagation of a localized instability in an inflated elastic tube. *Int. J. Solids Structures* 27 (1991) 1085–1111.
23. D. Lasry and T. Belytschko, Localization limiters in transient problems. *Int. J. Solids Structures* 24 (1988) 581–597.
24. J. Mandel, Conditions de stabilité et postulat de drucker. In: J. Kravtchenko and P.M. Sirieys (eds), *Rheology and Soil Mechanics.* Berlin: Springer (1966) pp. 58–68.

25. Z. Marciniak and K. Kuczynski, Limit strains in the process of stretch forming sheet metal. *Int. J. Mech. Sciences* 9 (1967) 609–625.
26. R.D. Mindlin, Micro-structure in linear elasticity. *Arch. Rat. Mech. Anal.* 16 (1964) 51–78.
27. R.D. Mindlin, Second gradient of strain and surface-tension in linear elasticity. *Int. J. Solids Structures* 1 (1965) 417–438.
28. A. Molinari and R.J. Clifton, Analytical characterization of shear localization in thermoviscoplastic solids. *J. Appl. Mech.* 54 (1987) 806–812.
29. J.R. Rice, The localization of plastic deformation. In: W.T. Koiter (ed.), *Theoretical and Applied Mechanics.* Proceedings of the 14th I.U.T.A.M. Conference, Delft, August 30–September 4, 1976. Amsterdam: North-Holland (1976) pp. 207–220.
30. E.S. Suhubi and A.C. Eringen, Nonlinear theory of micro-elastic solids–II. *Int. J. Engng. Sci.* 2 (1964) 389–404.
31. T.Y. Thomas, *Plastic Flow and Fracture in Solids.* New York: Academic Press (1961).
32. R.A. Toupin and D.C. Gazis, Surface effects and initial stress in continuum and lattice models of elastic crystals. In: R.F. Wallis (ed.), *Proceedings of the International Conference on Lattice Dynamics, Copenhagen, August 1963.* Oxford: Pergamon Press (1965) pp. 597–605.
33. N. Triantafyllidis and B.N. Maker, On the comparison between microscopic and macroscopic instability mechanisms in a class of fiber-reinforced composites. *J. Appl. Mech.* 52 (1985) 794–800.
34. N. Triantafyllidis and E.C. Aifantis, A gradient approach to localization of deformation. I. Hyperelastic materials. *J. Elasticity* 16 (1986) 225–237.
35. V. Tvergaard, A. Needleman and K.K. Lo, Flow localization in the plain strain tensile test. *J. Mech. Phys. Solids* 29 (1981) 115–142.
36. J.D. Van der Waals, The thermodynamic theory of capillarity under the hypothesis of a continuous variation of density (in Dutch). *Verhandel. Konink. Akad. Weten. Amsterdam (sec. 1)* 1 (1893).